Influence of fiber orientation on the ballistic performance of needlepunched nonwoven fabrics

Mechanics of Materials 94 (2016) 106–116

Contents lists available at ScienceDirect

Mechanics of Materials

journal homepage: www.elsevier.com/locate/mechmat

Influence of fiber orientation on the ballistic performance of needlepunched nonwoven fabrics

F. Martínez-Hergueta [a], A. Ridruejo [b], F. Gálvez [b], C. González [a,b], J. LLorca [a,b,*]

[a] IMDEA Materials Institute, C/Eric Kandel 2, 28906 Getafe, Madrid, Spain
[b] Department of Materials Science, Polytechnic University of Madrid, E. T. S. de Ingenieros de Caminos, 28040 Madrid, Spain

ARTICLE INFO

Article history:
Received 5 June 2015
Revised 10 November 2015
Available online 3 December 2015

Keywords:
Needlepunched nonwoven fabrics
Polypropylene
Fracture micromechanisms
Ballistic impact

ABSTRACT

The influence of the initial fiber orientation distribution on the ballistic performance of a needlepunched nonwoven polyethylene fabric was analyzed. To this end, ballistic tests were carried out in specimens pre-deformed along the machine or the transverse directions and the influence of pre-deformation on the fiber orientation was measured by means of wide angle X-ray diffraction. It was found that pre-deformation along the machine direction (the soft orientation of the fabric) led to more isotropic in-plane mechanical response and to a marked increase in the specific ballistic limit and in the energy dissipated by unit weight while the opposite behavior was found after stretching the fabric along the transverse direction. These differences were accompanied by changes in the penetration mechanics from extensive fiber pull-out to slippage between fibers in the network. These results highlight how the nature of the nonwoven microstructure (connectivity of the entanglement points and fiber orientation distribution) can be tailored to improve the impact performance.

1. Introduction

Nonwoven fabrics are structural materials made up by a disordered fiber network linked by local fiber bonds of different nature, such as simple mechanical entanglement, thermal fusion or chemical binders (Russell, 2007). As compared with standard woven fabrics, nonwoven textiles present lower stiffness and strength but much higher deformability and energy absorption capability. Moreover, the micromechanisms of deformation and failure are much more complex due to the randomness of the microstructure.

The initial studies of the structural performance of nonwoven fabrics were focused on paper (Bronkhorst, 2003; Hägglund and Isaksson, 2006; Isaksson et al., 2006, 2004) but more recent analyses have dealt with glass (Ridruejo et al., 2010), polyamide (Silberstein et al., 2012), polypropylene (Farukh et al., 2013; Jubera et al., 2014; Ridruejo et al., 2011, 2015) and polyethylene (Martínez-Hergueta et al., 2015; Raina and Linder, 2014; Raval et al., 2013) nonwoven fabrics. These investigations found that the micromechanisms of deformation and fracture depend on the interaction of a number of factors including fiber uncurling, bond failure and fiber reorientation as well as fiber sliding and fracture. Moreover, the nature of interfiber bonds (either brittle links induced by chemical forces or local fusion or entanglement knots) also changes dramatically the mechanical performance. Within this complex scenario, it is necessary to gain a deeper understanding of the influence of different microstructural factors (fiber orientation, bond density and nature, etc.) on the overall mechanical response to be able to design nonwoven fabrics with optimized properties.

Nonwoven fabrics manufactured with high performance aramid or polyethylene fibers have shown an excellent performance in ballistic protection (Russell et al., 2005; Chocron

* Corresponding author at: IMDEA Materials Institute, C/Eric Kandel 2, 28906 Getafe, Madrid, Spain, Department of Materials Science, Polytechnic University of Madrid, E. T. S. de Ingenieros de Caminos, 28040 Madrid, Spain. Tel.: +34 915 493422; fax: +34 915 503 047.
E-mail address: javier.llorca@upm.es, javier.llorca@imdea.org (J. LLorca).

http://dx.doi.org/10.1016/j.mechmat.2015.11.019
0167-6636/

et al., 2008; Wilusz, 2008). In particular, they show much better ballistic performance against small metallic fragments than their woven counterparts (Cheeseman and Bogetti, 2003; Thomas et al., 2003) and nonwoven fabric shields can provide the same protection against small fragments with one third of the areal weight as those based on dry woven fabrics (Ipson and Wittrock, 1966). Moreover, they have also been used to reduce damage during ballistic impact in combination with woven fabrics (Lin et al., 2009a, 2009b) or in sandwich structures (Lin et al., 2005; Shahdin et al., 2009). Nevertheless, very little is known about the influence of nonwoven fabric microstructure on the ballistic performance (Kang and Lee, 1999; Laible and Henry, 1971).

The main objective of this investigation is to provide fundamental insights on the influence of one critical microstructural parameter (fiber orientation) on the mechanical behavior under impact of a needlepunched nonwoven fabric that presents outstanding ballistic performance. Fiber orientation (and, thus, the in-plane mechanical response) was systematically modified by pre-stretching the fabric before the impact tests and the fiber orientation distribution was characterized by means of wide angle X-ray diffraction (WAXD). Finally, the influence of fiber alignment on the ballistic performance (in terms of the ballistic curve and the ballistic limit) was measured and discussed to the light of the deformation and failure micromechanisms.

2. Material

The material used in this investigation was a commercial needlepunched nonwoven fabric denominated Fraglight NW201 (DSM). It is manufactured by the continuous deposition of single filaments of Dyneema SK75 ultrahigh molecular weight polyethylene, of approximately 60 mm in length, on a moving bed surface, forming a batt. The batt is needle-felted with the aid of the oscillatory application of barbed needles producing fiber loops and mechanical entanglements among fibers (Russell, 2007). The nominal areal density and thickness of the fabric, as given by the manufacturer, were ≈190–220 g/m^2 and ≈1.5 mm, respectively.

The microstructure and in-plane mechanical properties of this material were analyzed in detail in a recent paper (Martínez-Hergueta et al., 2015). The manufacturing process introduces two principal material orientations, known as machine (MD) and transverse (TD) directions, which follow the bed displacement and the perpendicular orientation, respectively. While the initial fiber orientation was random and isotropic, the in-plane mechanical properties were highly anisotropic. The stiffness, strength and energy dissipated per unit volume upon deformation in the TD were 2–3 times higher than those along MD, while the strain at maximum load along TD was only one half of that along MD. This anisotropic behavior was dictated by the microstructure evolution. Fibers tended to be oriented along the loading direction when the fabric was deformed along TD but the fiber orientation distribution remained fairly isotropic during deformation along MD. Pull-out tests of multiple fibers showed that the structure of the knots connected more fibers along TD than along MD, leading to the anisotropic mechanical response. The better fiber interconnection along TD led to the contribution of a larger fraction of fibers, enhancing the mechanical response. In terms of affinity, fabrics deformed along TD essentially displayed affine deformation – i.e. most of the macroscopic strain was transferred to the fibers by the surrounding nonwoven – while MD-deformed fabrics underwent non-affine deformation, and most of the macroscopic strain was not transferred to the fibers.

3. Experimental techniques

3.1. Deformation before ballistic tests

Based on the previous results (Martínez-Hergueta et al., 2015), nonwoven specimens were deformed along TD and MD prior to the impact tests to modify systematically the initial fiber orientation distribution. To this end, rectangular samples of 500 mm in width and different heights were cut from the fabric roll by direct Joule's heating with a straight copper wire connected to a electrical power supply. They were attached to the actuator and the frame of an electromechanical universal mechanical testing machine (Instron 1122) by means of two flat steel plates fastened with screws to clamp the fabric by friction. The width of the grips was 300 mm, and a 100 mm free zone was unstressed at each side of the sample. Tests were carried out under stroke control at cross head speeds of 1 mm/s. The load was continuously recorded with a 25 kN load cell together with the cross-head displacement of the testing frame. All the samples, regardless of the initial length, were stretched up to a final length of 500 mm, so the final dimensions of the samples for the ballistic tests were 500 × 500 mm^2.

3.2. Wide angle X-ray diffraction

The fiber orientation distribution before and after deformation was measured by means of WAXD, following the methodology presented in Martínez-Hergueta et al. (2015). The Dyneema SK75 ultrahigh molecular weight polyethylene fibers are highly crystalline and the orthorhombic crystals are oriented parallel to the fiber axis (Russell et al., 2013). X-ray diffraction patterns provide information about the crystal (and, thus, the fiber) orientation in the nonwoven fabric.

WAXD patterns of as-received and deformed fabrics were acquired with a flat plate camera attached to a Philips 2 kW tube X-ray generator using monochromatic nickel-filtered Cu K_α radiation with $\lambda = 1.5$ Å wavelength. The scanning records were focussed in the diffraction angles of 2θ between 15° and 25° which encompass the diffraction peaks corresponding to (110) and (200) planes of the orthorhombic crystal. The spot size was around ≈1 mm^2 and the exposure time 1 min. It should be noticed that, although the spot size was much smaller than the fiber length, the orientation distribution functions obtained with this technique were in agreement with those obtained by 3D X-ray microtomography (Martínez-Hergueta et al., 2015).

The image treatment of the diffraction patterns was carried out by the software FIT2D. The intensity of the diffraction planes was measured for a certain angle in order to identify properly the position of the diffraction peaks with respect to the beam center. Orientation distribution functions (ODFs) of the fibers were computed by measuring a circular section of 30 pixels width around the main diffraction peak in 360 points homogeneously distributed in the planar area.

The equivalent intensity used for the comparison of the patterns was the result of the diffraction intensity minus the intensity of the background area to remove the influence of the different fiber volume or exposure time. Finally, all intensity curves were normalized to obtain an area equal to 1 under the ODF function. This image treatment was carried out for both diffraction planes, resulting in similar ODFs.

3.3. Differential scanning calorimetry

Differential scanning calorimetry of Dyneema fibers was carried out in nitrogen atmosphere using a TA Instruments Q200 apparatus. Prior to testing, each specimen was weighted (3–5 mg) and placed in an aluminium pan, sealed with an aluminium cover. The specimen temperature was stabilized at 20 °C for 10 min, and then heated at a rate of 10 °C/min up to 200 °C.

3.4. X-ray computed tomography

X-ray computed tomography (XCT) of the nonwoven fabric was carried out to ascertain the effect of pre-deformation on the fiber distribution. Tomograms were obtained with a Phoenix Nanotom 160 nF at 50 kV and 275 μA using a Mo target. 1700 radiographs were acquired for each tomogram using an exposure time of 750 ms. The tomograms were reconstructed from these radiographs through an algorithm based on the filtered back-projection procedure for Feldkamp cone beam geometry. The reconstructed volume encompassed a felt area of 5 × 5 mm^2 with a resolution of 3 μm/voxel.

3.5. Ballistic tests

As-received and pre-deformed fabrics of 500 × 500 mm^2 were clamped along their four edges using an aluminum rigid rig. 16 steel screws with 6 mm diameter were used to clamp the fabric to the frame. The four edges of the fabric were previously impregnated with Derakane 8084 epoxy vinylester resin to inhibit sliding. The resin was cured at room temperature for 24 h. The free surface of the fabric within the frame occupied 350 × 350 mm^2.

Impact tests were carried out with a pneumatic launcher SABRE A1 + gas gun. The projectile was a steel sphere with 5.5 mm in diameter (caliber 0.22) and 0.706 g of mass which was fit on a barrel of 7.62 mm in diameter using a sabot. The impact velocity was in the range 270–400 m/s, leading to impact energies between 25 and 55 J. A Phantom V12 high-speed video camera was used to measure the initial and residual velocities of the projectile and to obtain the energy absorbed by the fabric during impact. The images were recorded at a frame rate of 40,000 fps, a resolution of 512 × 256 pixels and an exposure time of 23.45 μs.

4. Experimental results

4.1. Pre-deformed specimens

Specimens of 500 mm in width (with 300 mm between grips) and different heights were deformed up a final length, l_f, of 500 mm. The initial length of the sample, l_0, was selected according to $l_0 = l_f/(1+\epsilon)$ so after stretching, the sample

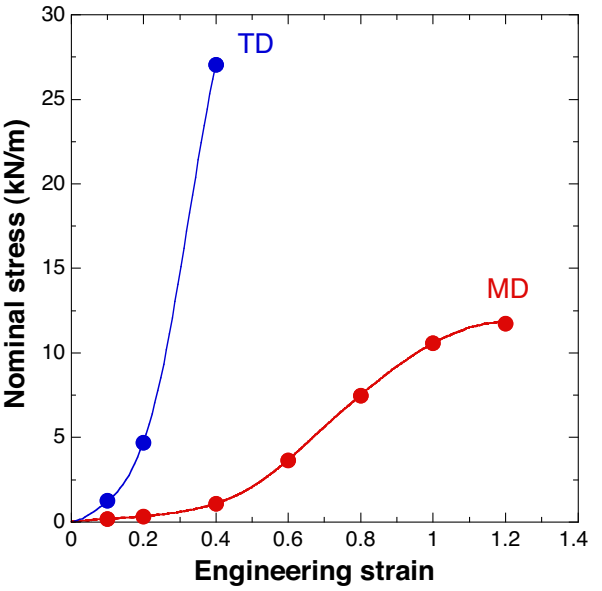

Fig. 1. Nominal stress vs. engineering strain curves of the specimens pre-deformed along TD and MD. The solid circles in each curve indicate the pre-deformation level of each sample.

was deformed up to an engineering strain ϵ of 10%, 20%, 40%, 60%, 80%, 100% or 120% along MD and up to 10%, 20% or 40% along TD. The corresponding nominal stress (force per unit width) vs. engineering strain curves for both orientations are plotted in Fig. 1 and they show the strong anisotropy in the mechanical response of the nonwoven fabric.

In all cases, the fabric was unloaded before the maximum load has been reached during the test, and thus before the onset of damage localization in a given region of the fabric appeared except in the case of the nonwoven fabric deformed 120% along MD. Tests with periodic unloading – reloading cycles were carried out in a previous investigation to ascertain the contribution of elastic and inelastic strains to the total deformation. It was found that most of the deformation was irrecoverable even at very low strains and the mechanical behavior of the nonwoven fabric was pseudo-plastic. Moreover, unloading neither modified the network structure nor contributed to damage (Martínez-Hergueta et al., 2015).

The shape of the specimens (in which the width was much longer that the initial height) and the smaller width of the grips (as compared with the specimen width) reduced the transversal contraction of the needlepunched fabric during tensile deformation (Fig. 2). As a result, the central region of the sample was subjected to a homogeneous strain along the loading direction and was not influenced by the lateral contraction. Thus, the microstructure evolution as a result of stretching could be considered homogeneous in this central region, leading to a constant reduction of the areal density as well. Under this hypothesis, and taking into account that the deformation of the nonwoven fabric is pseudo-plastic (Martínez-Hergueta et al., 2015), the areal density, ρ, in the central region of the deformed specimens can be computed as

$$\rho = \frac{\rho_0}{1+\epsilon} \tag{1}$$

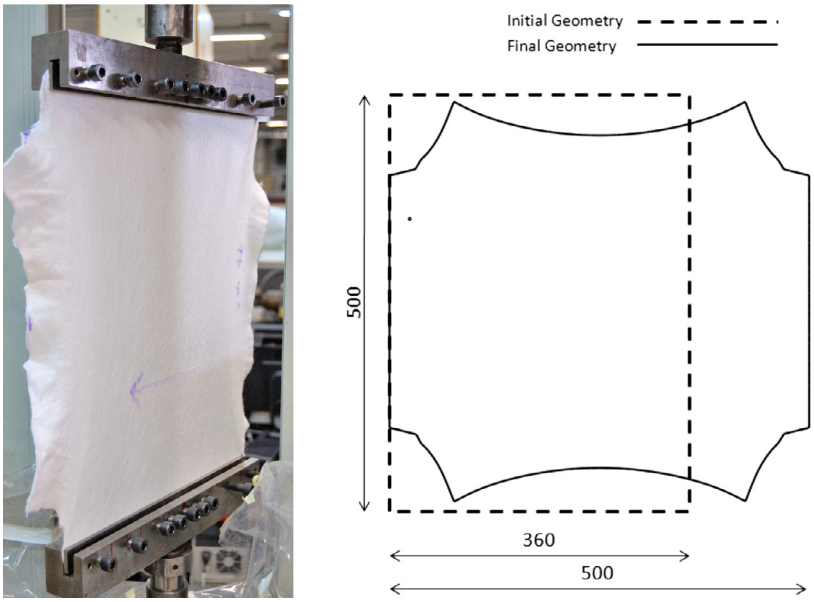

Fig. 2. (a) Specimen tested up to 40% engineering strain along TD. (b) Schematic of the geometry of the specimen before and after 40% deformation along TD.

where $\rho_0 = 200\ \mathrm{g/m^2}$ was the areal density of the as-received material.

The microstructure evolution in the central region of the stretched specimens was characterized by means of the fiber ODF obtained by WAXD in order to assess whether it was homogeneous. WAXD patterns were obtained at four different positions of the specimen deformed up to 40% along TD, which are indicated in Fig. 3(a). The corresponding fiber ODFs are plotted in Fig. 3(b) together with that of an isotropic material. The fiber distribution in the as-received material was isotropic (Martínez-Hergueta et al., 2015) while the fibers were aligned with respect to TD in the central region of the samples deformed by 40% in this direction. The differences among the spots b, c and d were negligible, supporting the assumption that the deformation in the central region of the specimen was homogeneous, while the fiber ODF corresponding to the spot a, which was within the region unconstrained by the grips, was different. Thus, a central region of $350 \times 350\ \mathrm{mm^2}$ presented a homogeneous microstructure with the same areal density and fiber ODF.

The diffraction patterns of the central region of two samples stretched along perpendicular directions (MD and TD) are depicted in Fig. 4(b) and (c), respectively. The corresponding ODFs are shown in a polar representation in Fig. 4(a). They show that fibers were aligned in the loading direction in each case. It is also worth noting that the degree of orientation was very similar in both cases although the sample was stretched up to 40% along TD and up to 100% along MD. These deformations are close to the maximum value that can be attained in each direction before the onset of damage localization (Martínez-Hergueta et al., 2015) and points out the anisotropic behavior of the needlepunched nonwoven fabric. Although the initial fiber ODF is isotropic, the mechanical behavior of the nonwoven along MD and TD is anisotropic and this is reflected in the evolution of the fiber ODF: much more fibers contribute to carry the load along TD, leading to a stiffer and stronger mechanical response, as compared with MD.

The evolution of the microstructure with respect to the strain level was also analyzed by WAXD in both orientations, and the results along MD are plotted in Fig. 5. The fibers were progressively oriented with the applied strain along the $\pi/2$ and $-\pi/2$ directions and reached a maximum for an applied strain of 100%. Further straining up to 120% led to a reduction in anisotropy of the fiber ODF, which also became asymmetric because of the onset of damage. Similar results were obtained along TD but they are not plotted for the sake of brevity.

4.2. Deformation and failure mechanisms under impact

Ballistic impacts were carried out in as-received and predeformed specimens. The deformation of the as-received nonwoven fabric during impact at 305 m/s (below the ballistic limit) and at 360 m/s (above the ballistic limit) is shown in Figs. 6 and 7, respectively. Energy dissipation during impact was due to the transfer of momentum from the projectile to the fabric and to the strain energy dissipated by the fabric. The in-plane longitudinal wave traveling through the nonwoven made the fibers move radially towards the impact point, leading to the formation of a conical region of strained material. The deformation in this region was accommodated by the same mechanisms observed during in-plane tensile deformation, which included uncurling and stretching of the active fibers connected by the entanglement points followed by fiber sliding and pull-out from the entanglement points, leading to a permanent global deflection of the target until the projectile was stopped (Fig. 6).

In contrast with the ballistic performance of woven fabrics (Chocron et al., 2010), the nonwoven counterparts showed a much larger out-of-plane deformation, which comes as a result of the lower stiffness and higher strain to

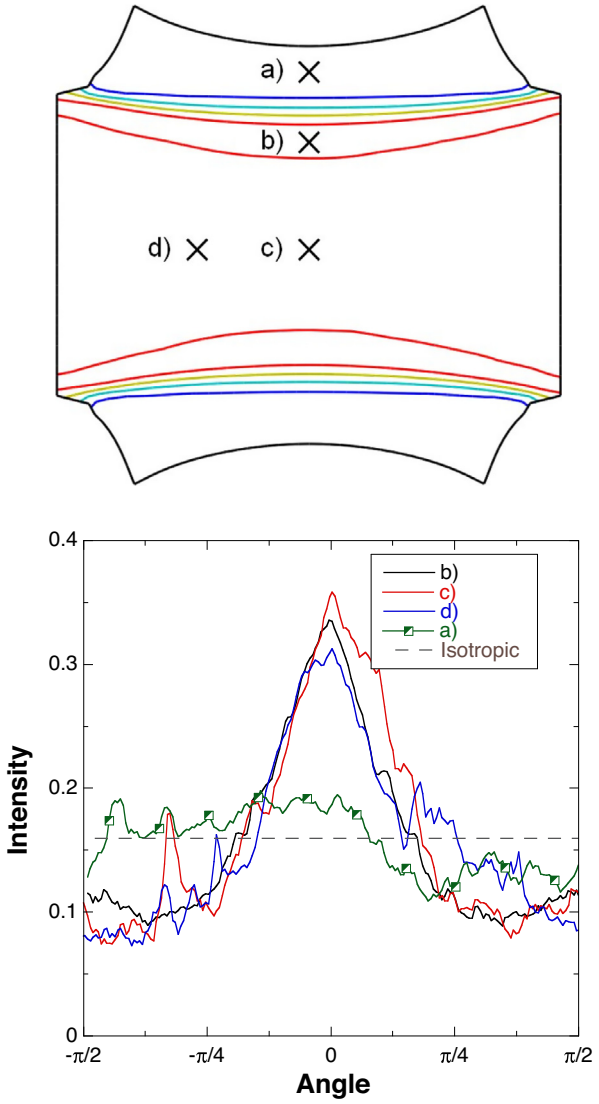

Fig. 3. (a) Position of the spots scanned by WAXD in the sample deformed up to 40% along TD. (b) Fiber orientation distribution function of the spots indicated in (a). The horizontal line stands for the theoretical fiber ODF of an isotropic material, which is very close to that of the as-received fabric.

failure. The base of the cone was not circular but elliptical due to the different stiffness of the nonwoven fabric along TD and MD. It should be noted that the stiffness of the material (and, thus, the wave propagation speed) varied with the applied strain and the orientation. For instance, Chocron et al. (2002) reported an approximately linear increase in the wave propagation velocity in these materials from 600 m/s of the as-received condition up to 4000 m/s after 25% of stretching.

In the tests carried out above the ballistic limit, the final penetration of the target was accomplished by tearing as the fibers were pulled out from the entanglement points or broken near to the impact point (Fig. 7). It should be noted that fiber fracture was not found to be a dominant fracture mechanism during quasi-static in-plane tensile deformation (Martínez-Hergueta et al., 2015). Thermal softening of the Dyneema fibers, due to adiabatic heating, may be responsible for fiber fracture during impact. To check this hypothesis, as-received fibers (carefully extracted from the nonwoven fabric with tweezers) and fibers attached to the projectile after the impact were analyzed by means of differential scanning calorimetry. In the case of the fibers attached to the projectile, the whole fiber was analyzed (average length ≈60 mm) although only a small part of the fiber was in contact with the projectile of 5.5 mm in diameter.

The thermograms of the as-received and impacted fibers are shown in Fig. 8. The melting enthalpy of the as-received and impacted fibers were 293 J/g and 204 J/g, respectively. Taking into account that the higher melting enthalpy, the higher crystallinity, these results point to a local melting of the fiber during impact. The ratio between the peaks at 147 °C and 156 °C varied significantly among impacted samples, mainly due to the heterogeneous temperature profile during impact as well as during cooling after the impact fiber. Nevertheless, the thermogram clearly indicates that impacted fibers were heated at temperatures higher than 160 °C, leading to the partial melting of the fiber. It should be noted that this phenomenon was only found in fibers extracted from specimens that underwent penetration.

4.3. Ballistic performance

The ballistic performance of the as-received and pre-deformed nonwoven fabric was assessed in terms of the ballistic curves depicted in Fig. 9(a), (b) and (c). The solid and broken lines in these figures correspond to the Lambert formula

$$V_{residual} = (V_{initial}^{n} - V_{50}^{n})^{1/n} \tag{2}$$

where the ballistic limit V_{50} and the exponent n were obtained for each set of experimental results by the least squares fitting. The best fit to the experimental data was obtained with $n = 5$ for the as-received and the specimens pre-deformed along TD and with $n = 3$ for the specimens pre-deformed along MD. It should be noted that the gas gun did not allow to launch projectiles with speeds lower than 250 m/s. If the ballistic limit was above this speed, the experimental values were in very good agreement with V_{50} in Eq. (2). Four specimens (those pre-deformed along TD by 20% and 40% and along MD by 100% and 120%) presented a ballistic limit below 250 m/s that could not be reached experimentally. In these cases, the ballistic limit was given by V_{50}, as obtained by the fitting of Eq. (2) to the available experimental results.

Regardless of the scatter of the experimental data in Fig. 9, it is obvious that pre-deformation of the nonwoven fabric along TD led to a marked reduction in the ballistic performance, Fig. 9(a). Similar results were obtained when the nonwoven fabric was pre-deformed more than 60% along MD, Fig. 9(c), but pre-deformation by 10% or 20% along MD did not degrade the ballistic performance within the experimental scatter, Fig. 9(b). A clearer view of the effect of pre-deformation on the ballistic performance can be found in Fig. 10(a), in which the ballistic limit V_{50} of the as-received and pre-deformed samples is plotted as a function of the areal density, determined according to Eq. (1). Pre-deformation of the fabrics led to a reduction in the

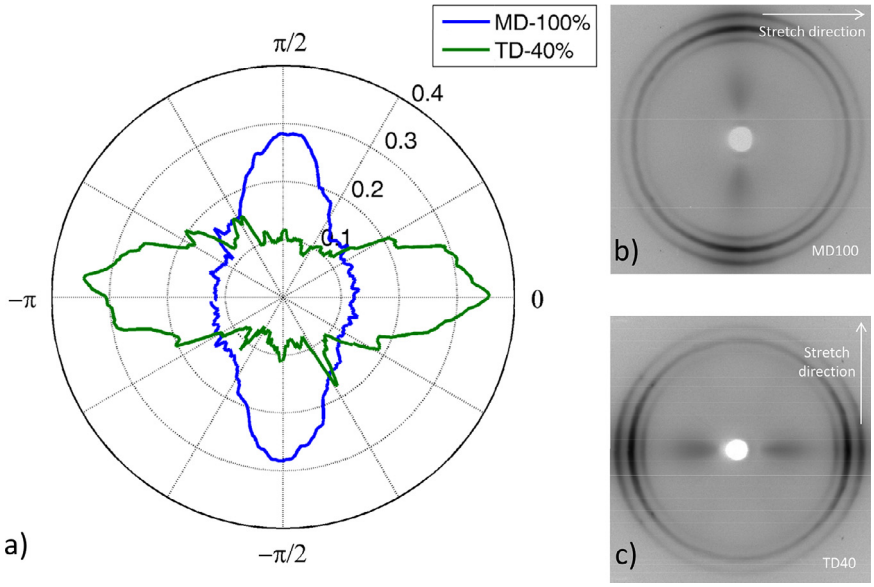

Fig. 4. (a) Polar representation of the fiber ODF after 100% deformation along MD and 40% deformation along TD. (b) 2D WAXD pattern of a sample deformed 100% along MD. (c) 2D WAXD pattern of a sample deformed 40% along TD.

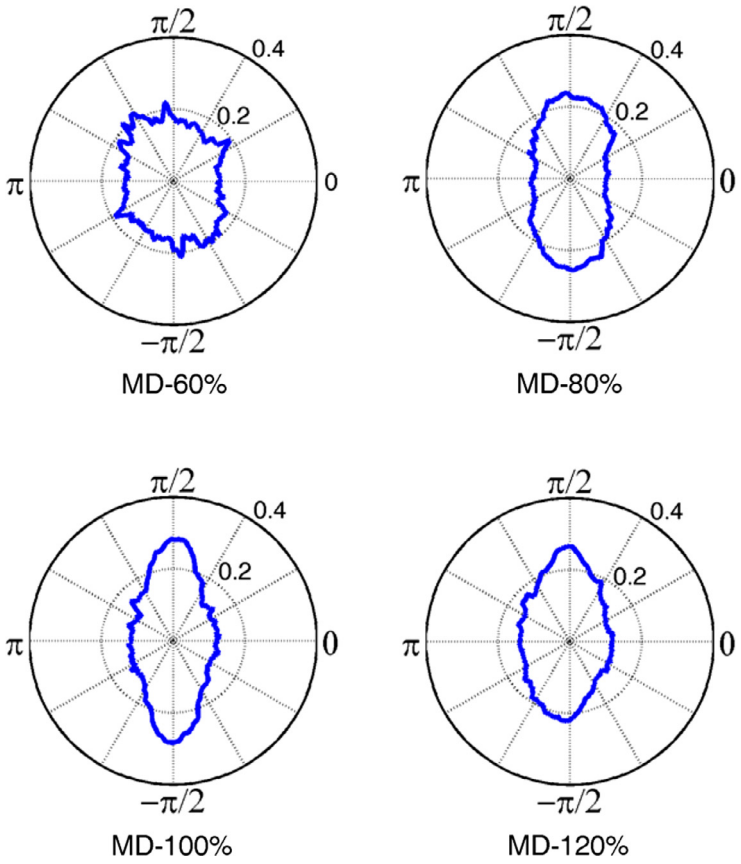

Fig. 5. Polar representation of the fiber ODF as a function of the applied strain along MD.

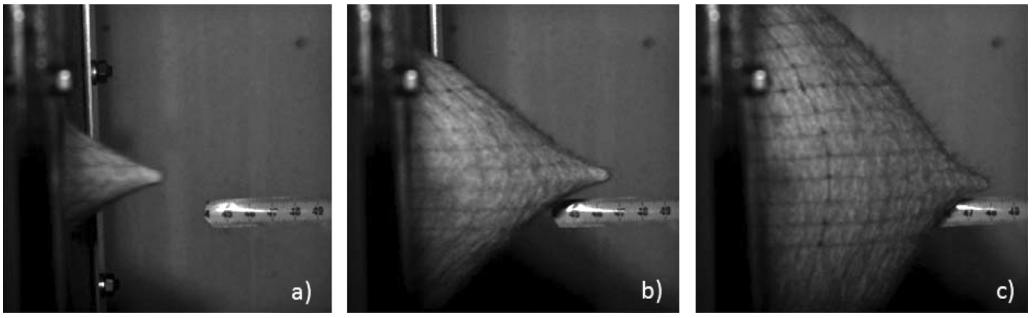

Fig. 6. Deformation of the as-received nonwoven fabric during impact at 305 m/s. (a) $t = 200$ μs, (b) $t = 900$ μs and (c) $t = 2150$ μs. The projectile is stopped by the fabric.

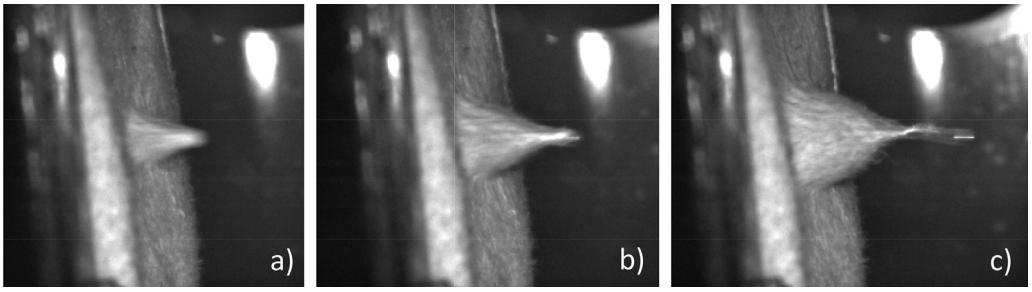

Fig. 7. Deformation of the as-received nonwoven fabric during impact at 360 m/s. (a) $t = 50$ μs, (b) $t = 100$ μs and (c) $t = 175$ μs. The projectile penetrates the fabric.

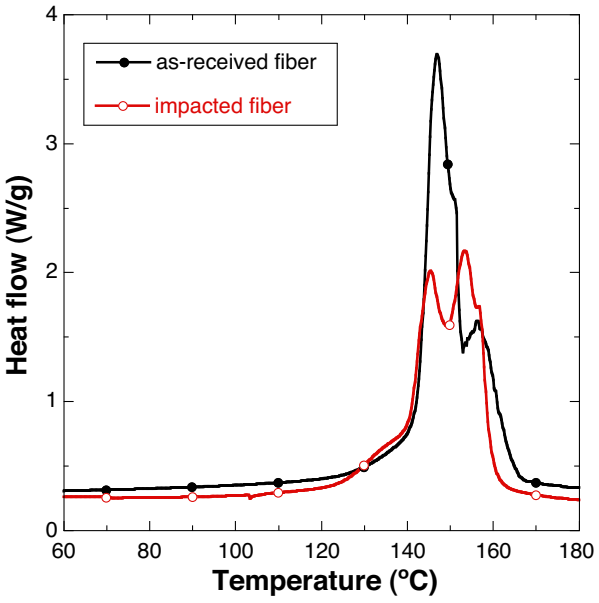

Fig. 8. Differential scanning calorimetry thermograms of as-received and impacted fibers.

ballistic limit approximately linear with the areal density for both MD and TD. However, the reduction was higher for the specimens pre-deformed along TD. It should be noted, however, that the specific ballistic limit, V_{50}/ρ, increased from 1.7 m^3/gs to 2.6 m^3/gs when the fabric was stretched by 100% along MD, and decreased slightly (up to 1.7 m^3/gs) after 40% deformation along TD, Fig. 10(b). As indicated above, ballistic impact on the nonwoven fabric led to the formation of a cone of deformed material whose cross-section was elliptical. The ratio between the major and minor semi-axes of the ellipse, a/b, was measured for all the specimens that underwent penetration and the average value (together with the standard deviation) is plotted in Fig. 10(b) as a function of the pre-deformation of the fabric. a/b was ≈2 in the as-received fabric, increased up to ≈3.5 when the fabric was pre-deformed by 40% along TD and decreased up to ≈1.2 when the fabric was pre-deformed along MD by 80%. Further pre-deformation along MD did not modify the aspect ratio of the ellipse. These results point out again the influence of the fiber orientation and of in-plane isotropy in the mechanical properties on the ballistic performance. In this respect, it should be noted that stretching along MD from 100% to 120% modified neither the fiber orientation (Fig. 5), nor the shape of the elliptical zone that contributed to the deformation, nor the specific ballistic limit, Fig. 9(b).

Thus, fiber orientation by pre-deformation along MD and TD had different effects on the specific ballistic limit and on the energy absorbed per unit mass of the fabric and they have to be traced to changes in the dominant deformation and fracture mechanisms. The deformation during impact of the nonwoven fabrics pre-deformed along MD by 60% and along TD by 20% is depicted in Figs. 11 and 12, respectively. Both cases correspond to impact tests at speeds above the ballistic limit that led to full penetration of the fabric by the projectile. The impact gave rise to the formation of a cone of strained fabric in both cases but the final fracture of the specimen pre-deformed along MD was accompanied by extensive fiber pull-out, Fig. 11(c), which was not found

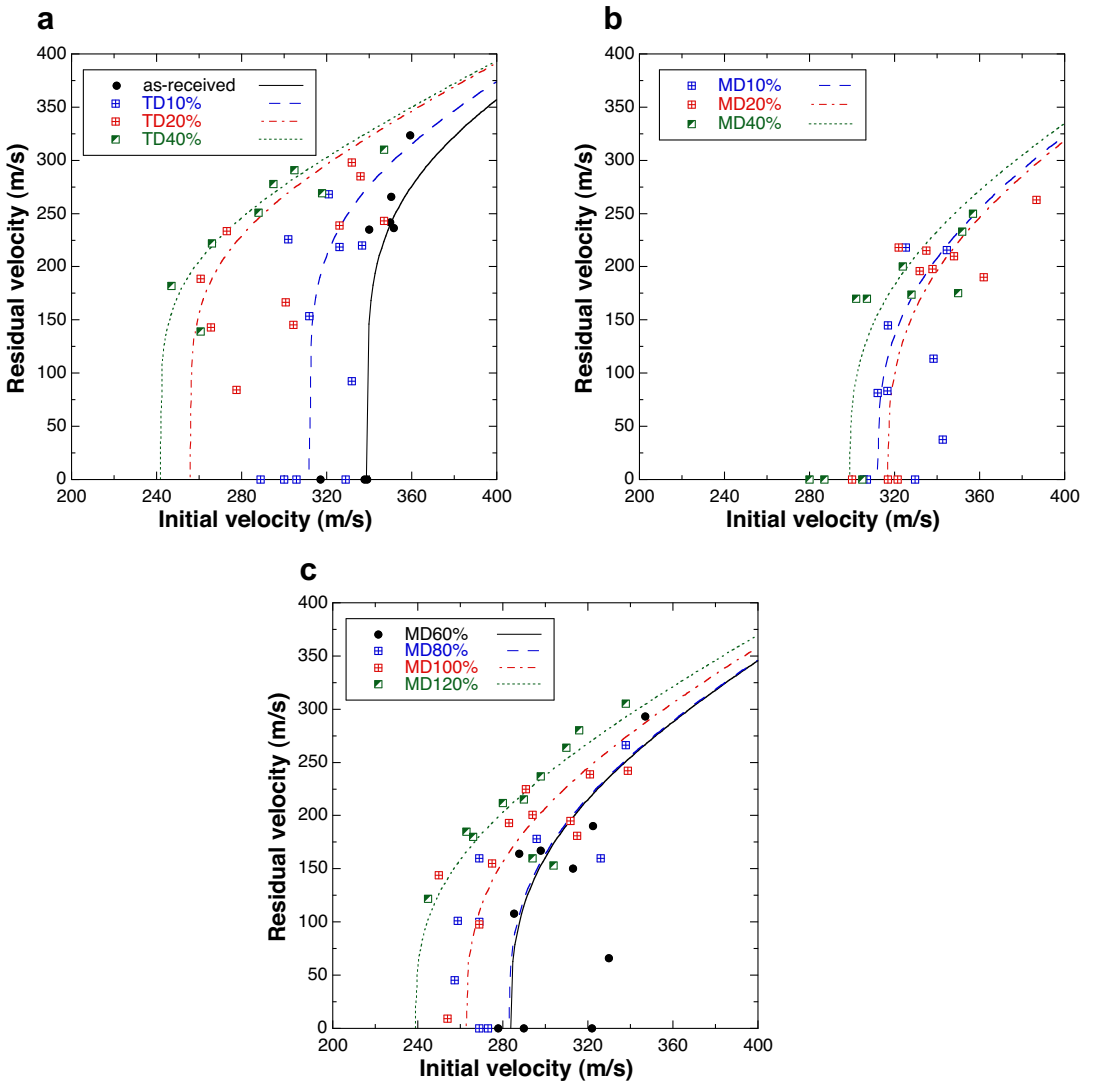

Fig. 9. Experimental results of the ballistic impact tests for the nonwoven fabric. (a) As-received nonwoven fabric and specimens pre-deformed along TD by 10%, 20% and 40%. (b) Specimens pre-deformed along MD by 10%, 20% and 40 %. (c) Specimens pre-deformed along MD by 60%, 80% 100% and 120%. The solid and broken lines stand for Eq. (2) for each set of experimental results.

in the sample pre-deformed along TD, Fig. 12(c). Fiber pull-out from the fabric was identified as one the most important energy absorption mechanisms during in-plane deformation of the needlepunched nonwoven fabric Martínez-Hergueta et al. (2015) and was responsible for the changes in the ballistic behavior between the specimens stretched along MD and TD.

These changes in the failure mechanisms can be traced to the anisotropic deformation of the nonwoven fabric along TD and MD, which led to different mechanical responses under impact. Pre-deformation of the fabric along TD was accompanied by the preferential orientation of the fibers along the loading direction, Fig. 4(a) and (c). The resulting microstructure can be found in the tomograms obtained by XCT in Fig. 13. The as-received material presents an isotropic fiber orientation, Fig. 13(a), but most of the fibers have been oriented along TD after 40% deformation along this orientation, Fig. 13(b). As a result, the mechanical anisotropy of the nonwoven fabric is maximum because very few fibers remain oriented along MD. During impact, the projectile was able to slip through the fibers because the resistance to deformation along MD was negligible, and the overall energy absorption capability decreased. On the contrary, the fiber ODF was isotropic after pre-deformation along MD by 60% because most of the macroscopic strain was not transferred to the fibers in this orientation. Further straining led to preferred fiber alignment along MD, indicating that the entanglement points became effective to transfer the load to the fibers and, thus, the in-plane mechanical behavior of the fabric was more isotropic. This statement is supported by the almost circular shape of the elliptical zone that contributed to the deformation during impact, Fig. 10(b). The resistance to the impact was similar along MD and TD, and penetration took place by fiber pull-out from the

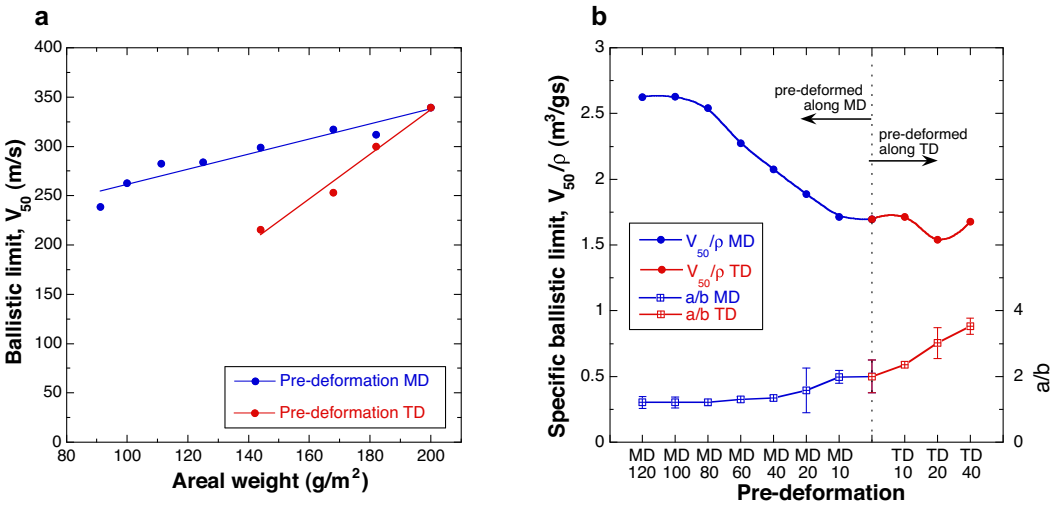

Fig. 10. (a) Ballistic limit, V_{50} of the nonwoven fabric as a function of the areal density, ρ. (b) Specific ballistic limit, V_{50}/ρ and aspect ratio (a/b) of the deformed region after impact in the specimens pre-deformation along MD and TD directions.

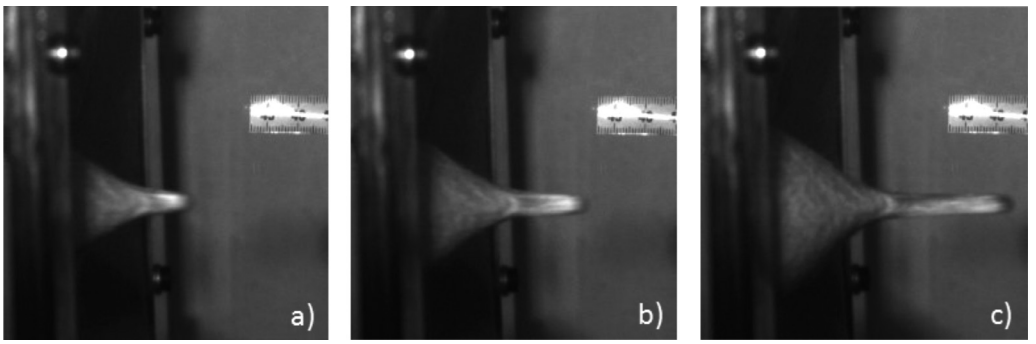

Fig. 11. Deformation of the nonwoven fabric pre-deformed 60% along MD during impact at 322 m/s. (a) $t = 150$ μs, (b) $t = 225$ μs and (c) $t = 350$ μs. Notice the large volume fraction of fibers pulled out from the fabric after penetration.

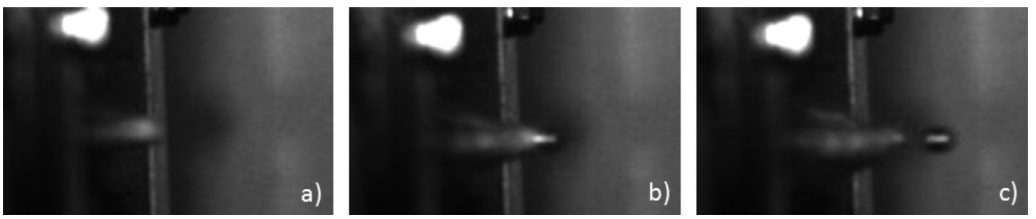

Fig. 12. Deformation of the nonwoven fabric pre-deformed 20% along TD during impact at 260 m/s. (a) $t = 75$ μs, (b) $t = 125$ μ and (c) $t = 175$ μs.

entanglement points rather than by slippage through the fiber network.

5. Conclusions

The impact behavior of a needle-punched nonwoven fabric was analyzed after stretching the fabric along TD and MD to ascertain the effect of the fiber orientation on the ballistic properties. While the initial fiber ODF was isotropic, the in-plane mechanical properties of the fabric were anisotropic because the structure of the knots connected more fibers along TD than along MD. In terms of affinity, TD-oriented fibers basically displayed affine deformation – i.e. most of the macroscopic strain was transferred to the fibers by the surrounding nonwoven – while MD-oriented fibers underwent non-affine deformation, and most of the macroscopic strain was not transferred to the fibers.

During impact, the energy of the projectile was accommodated by the formation of a cone of deformed material with an elliptical cross-section due to the different wave propagation speed along MD and TD. Energy dissipation during impact was due to the transfer of momentum from the projectile to the fabric and to the strain energy dissipated by the fabric due to the in-plane deformation. The deformation was accommodated by the same mechanisms observed during in-plane tensile deformation, which included uncurling and

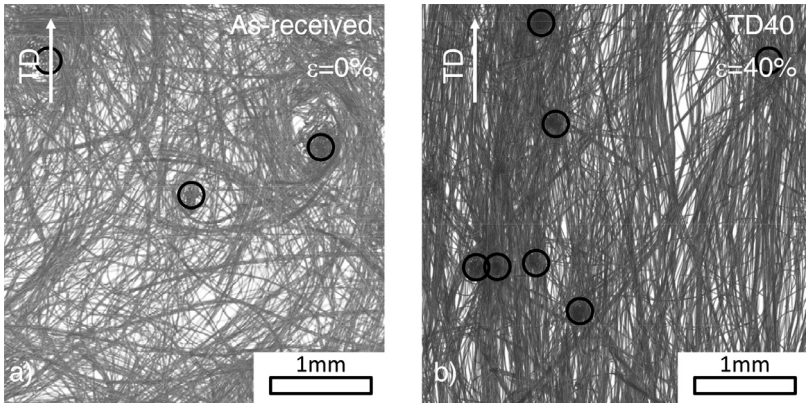

Fig. 13. XCT images of the needle-punched nonwoven fabric. (a) As-received condition. (b) After 40% deformation along TD, showing the preferential fiber orientation along TD. The entanglement points are marked with black circles.

stretching of the active fibers connected by the entanglement points followed by fiber sliding and pull-out, leading to a permanent global deflection of the target until the projectile was stopped.

The impact mechanisms in the pre-deformed specimens were similar but it was found that pre-stretching the nonwoven fabric along MD (the soft direction) up to 100% led to a continuous increase in the specific ballistic limit (minimum penetration velocity divided by the areal density) of the fabric and of the energy dissipated per unit weight. On the contrary, both the specific ballistic limit and the energy dissipated per unit weight decreased when the nonwoven fabric was pre-deformed along TD. Moreover, the elliptical zone of deformed material around the impact point became close to a circle when the fabric was pre-deformed along MD, while the aspect ratio of the ellipse increased if the material had been pre-deformed along TD. Penetration in the former situation (pre-deformation along MD) was accompanied by extensive fiber pull-out around the projectile but this phenomenon was not observed in the latter. Pre-deformation of the fabric along TD was accompanied by the preferential orientation of the fibers along the loading direction, enhancing the mechanical anisotropy of the nonwoven fabric because very few fibers remained oriented along MD. During impact, the projectile was able to slip through the fibers because the fabric resistance to deformation along MD was negligible and the overall energy absorption capability decreased. On the contrary, pre-deformation along MD led to a more isotropic in-plane mechanical behavior of the fabric, which improved the impact resistance as the projectile could not slip between fibers, which had to be pulled out from the fabric. These results show that careful design of the nature of the entanglement points and of the fiber orientation can be used to design nonwoven fabrics with improved energy absorption capability by maximizing energy dissipation by fiber pull-out and avoiding projectile penetration by slippage among fibers.

Acknowledgments

This investigation was supported the Spanish Ministry of Economy and Competitiveness through the projects TARGET (CENIT program, CDTI) and BIA2014-54916-R. FMH acknowledges the support of the Spanish Ministry of Education through the fellowship FPU12/02087. In addition, the assistance of J. P. Fernández (IMDEA Materials Institute) and E. Pérez (Instituto de Polímeros, CSIC) to carry out the WAXD analysis, and the collaboration of F. Sket and M.J. Pérez-Martín to accomplish the XCT experiments and the ballistic tests, respectively, are gratefully acknowledged.

References

Bronkhorst, C.A., 2003. Modelling paper as a two-dimensional elastic-plastic stochastic network. Int. J. Solids Struct. 40, 5441–5454.
Cheeseman, B.A., Bogetti, T.A., 2003. Ballistic impact into fabric and compliant composite laminates. Compos. Struct. 61, 161–173.
Chocron, S., Figueroa, E., King, N., Kirchdoerfer, T., Nicholls, A.E., Sagebiel, E., Weiss, C., Freitas, C.J., 2010. Modeling and validation of full fabric targets under ballistic impact. Compos. Sci. Technol. 70 (13), 2012–2022.
Chocron, S., Gálvez, F., Pintor, A., Cendón, D., Roselló, C., 2002. Characterization of Fraglight Non-woven Felt and Simulation of FSP's Impact in It. Final Report for the European Research Office of the US Army. Universidad Politécnica de Madrid.
Chocron, S., Pintor, A., Gálvez, F., Roselló, C., Cendón, D., Sánchez-Gálvez, V., 2008. Lightweight polyethylene non-woven felts for ballistic impact applications: material characterization. Compos. Part B Eng. 39, 1240–1246.
Farukh, F., Demirci, E., Sabuncuoglu, B., Acar, M., Pourdeyhimi, B., Silberschmidt, V.V., 2013. Characterisation and numerical modelling of complex deformation behaviour in thermally bonded nonwovens. Comput. Mater. Sci. 71, 165–171.
Hägglund, R., Isaksson, P., 2006. Analysis of localized failure in low-basis weight paper. Int. J. Solids Struct. 43, 5581–5592.
Ipson, T.W., Wittrock, E.P., 1966. Response of Non-Woven Synthetic Fiber Textiles to Ballistic Impact. Technical Report, No. tr-67-8-cm. Denver Research Institute.
Isaksson, P., Gradin, P., Kulachenko, A., 2006. The onset and progression of damage in isotropic paper sheets. Int. J. Solids Struct. 43, 713–726.
Isaksson, P., Hägglund, R., Gradin, P., 2004. Continuum damage mechanics applied to paper. Int. J. Solids Struct. 41, 4731–4755.
Jubera, R., Ridruejo, A., González, C., LLorca, J., 2014. Mechanical behavior and deformation micromechanisms of polypropylene nonwoven fabrics as a function of temperature and strain rate. Mech. Mater. 74, 14–25.
Kang, T.J., Lee, S.H., 1999. Characterization of reinforcing web structures in needle punched nonwoven composites. J. Compos. Mater. 33, 2116–2132.
Laible, R.C., Henry, M.C., 1971. Development of Ballistic Needle-Punched Felts. Technical Report, 60(4), 36. U.S. Army Natick Laboratories.
Lin, C.C., Huang, C.C., Chen, Y.L., Lou, C.W., Lin, C.M., Hsu, C.H., Lin, J.H., 2009a. Ballistic-resistant stainless steel mesh compound nonwoven fabric. Fibers Polym. 9, 761–767.
Lin, C.C., Lin, C.M., Huang, C.C., Lou, C.W., Meng, H.H., Hsu, C.H., Lin, J.H., 2009b. Elucidating the design and impact properties of composite nonwoven fabrics with various filaments in bulletproof vest cushion layer. Text. Res. J. 79, 268–274.

Lin, J.H., Hsu, C.H., Meng, H.H., 2005. Process of preparing a nonwoven/filament/woven-fabric sandwich structure with cushioning effect of ballistic resistance. Fibres Text. 13, 43–47.
Martínez-Hergueta, F., Ridruejo, A., González, C., LLorca, J., 2015. Deformation and energy dissipation mechanisms of needle-punched nonwoven fabrics: a multiscale experimental analysis. Int. J. Solids Struct. 64-65, 120–131.
Raina, A., Linder, C., 2014. A homogenization approach for nonwoven materials based on fiber undulations and reorientation. J. Mech. Phys. Solids 65, 12–34.
Raval, A., Patel, S.K., Kumar, V., Saraswat, H., Sayeed, M.A., 2013. Damage analysis and notch sensitivity of hybrid needlepunched nonwoven materials. Text. Res. J. 83, 1103–1112.
Ridruejo, A., González, C., LLorca, J., 2010. Damage micromechanisms and notch sensitivity of glass-fiber non-woven felts: an experimental and numerical study. J. Mech. Phys. Solids 58, 1628–1645.
Ridruejo, A., González, C., LLorca, J., 2011. Micromechanisms of deformation and fracture of polypropylene nonwoven fabrics. Int. J. Solids Struct. 48, 153–162.
Ridruejo, A., Jubera, R., González, C., LLorca, J., 2015. Inverse notch sensitivity: Cracks can make nonwoven fabrics stronger. J. Mech. Phys. Solids 77, 61–69.
Russell, B.P., Karthikeyan, K., Deshpande, V.S., Fleck, N.A., 2013. The high strain rate response of ultra high molecular-weight polyethylene: from fibre to laminate. Int. J. Impact Eng. 60, 1–9.
Russell, S., 2007. Handbook of Nonwovens. The Textile Institute, Woodhead Publishing Ltd, Cambridge, UK.
Russell, S., Pourmohammadi, A., Ezra, I., Jacobs, M., 2005. Formation and properties of fluid jet entangled HMPE impact resistant fabrics. Compos. Sci. Technol. 65, 899–907.
Shahdin, A., Mezeix, L., Bouvet, C., Morlier, J., Gourinat, Y., 2009. Fabrication and mechanical testing of glass fiber entangled sandwich beams: a comparison with honeycomb and foam sandwich beams. Compos. Struct. 90, 404–412.
Silberstein, M.N., Pai, C.-L., Rutledge, G.C., Boyce, M.C., 2012. Elastic-plastic behavior of non-woven fibrous mats. J. Mech. Phys. Solids 60, 295–318.
Thomas, H.L., Bhatnagar, A., Wagner, L.L., 2003. Needle-punched non-woven for high fragment protection. In: Proceedings of the 14th International Conference of Composite Materials. San Diego, California.
Wilusz, E., 2008. Non-Woven Fabrics for Military Applications. The Textile Institute, Woodhead Publishing Ltd, Cambridge, UK.